Electronic Supplementary information

Qualifying label components for effective biosensing by advanced high-throughput SEIRA methodology

Andrea Hornemann[a]*, Diane Eichert[b], Sabine Flemig[b], Gerhard Ulm[a], Burkhard Beckhoff[a]

[a] Physikalisch-Technische Bundesanstalt, Abbestr. 2-12, 10587 Berlin, Germany
[b] Elettra-Sincrotrone Trieste S.C.p.A. di interesse nazionale, Strada Statale 14,
  34149 Trieste, Italy
[c] BAM Bundesanstalt für Materialforschung und –prüfung, Richard-Willstätter-
 Str.10, 12489 Berlin, Germany

*Author for correspondence: Dr. Andrea Hornemann, Physikalisch-Technische Bundesanstalt, Abbestr. 2-12, 10587 Berlin, Germany

andrea.hornemann@ptb.de

Tel. +4930 3481 7183

Fax. +4930 3481 7103

Comparison between SERS and SEIRA

The enhancement factor [1] of SERS ranges from 10^6 to 10^{10}, and the Raman cross section ranges from about 10^{-31} to 10^{-29} cm^2/molecule [2], thus resulting in effective SERS cross sections of 10^{-23} cm^2/molecule to 10^{-22} cm^2/molecule (or: 10^{-21} cm^2/molecule to 10^{-19} cm^2/molecule), respectively. The enhancement factors for SEIRA are in the range of about 10^1 to 10^4 [3], and are leading to a similar or even somewhat higher speciation sensitivity as the average cross-section for infrared absorption is about nine orders of magnitude higher than in the optical range (from 10^{-22} cm^2/molecule to 10^{-20} cm^2/molecule) [3], thus resulting in an effective SEIRA cross section from about 10^{-24} cm^2/molecule to 10^{-22} cm^2/molecule (or: 10^{-21} cm^2/molecule to 10^{-19} cm^2/molecule), respectively.

An estimate for the bioassay detection limit with SEIRA readout can be derived from a comparison with typical SERS readout values providing that the biolabel binding mechanisms are somewhat similar. Taking into account now both the typical SERS detection limit range being located in the fmol to pmol range, and, in addition, the ratio of typical SERS to SEIRA enhancement factors being about 10^3, the typical SEIRA detection limit range can be estimated to be in the pmol to nmol range [5].

Comparison between conventional FTIR and SEIRA

While conventional FTIR presents the advantage of significantly probing a molecule signal with high sensitivity, SEIRA averages between 10 and 50 times the sensitivity of FTIR. The large advantage of SEIRA over FTIR however is the economy of time spent collecting the measurement. For SEIRA, only a handful of scans are needed, and not long acquisition (the S/N ratio is orders of magnitude lower with FTIR), which is an asset to collect structural information extremely rapidly and ultimately to monitor in-situ or online some biological process. In addition, molecules on metal surfaces show IR absorption 10–1500 times more intense than would be expected from conventional measurements without the metals[4, 5].

Inherent to the SEIRA technique compared to conventional FTIR is the metal surface influence that may lead to some spectral shapes, shifts and changes in intensities[6].

*Further details on **Material and methods***

Reagents

For the preparation of colloidal suspensions of Au NP in water, gold (III) chloride trihydrate (99.9%, Sigma-Aldrich), and trisodium citrate dihydrate (99%, Merck) were employed. For all experimental procedures, ultrapure water (18 MΩ·cm^{-1}, MicroLab UV, TKA GmbH) was applied. For the preparation of Au NP immobilized on MIR slides (KevleyTechnologies, USA), (3-Aminopropyl) trimethoxysilane (APTMS, 97%, Alfa Aesar) was used. Goat Anti-Mouse IgG (lot no. ABN-PAB9354-L002, Biozol, Germany) was employed for preparation of fluorophore-labeled antibody conjugates. The antigen Mouse Anti-Goat IgG (lot no. 6158-01, Biozol, Germany) was purchased in batch, predissolved at a concentration of 0.5 mg/ml in borate buffered saline (100 mM, pH~8.2). The flurophores Rhodamine B isothiocyanate (RITC, >70%, Sigma-Aldrich), Fluorescein 5(6)-isothiocyanate (FITC, ≥90%, Sigma-Aldrich) and Sulforhodamine B (SULFO, 75%, Sigma) were utilized for the coupling procedures. N, N-Dimethylformamide (DMF, 99.8%, Sigma-Aldrich) and sodium bicarbonate buffer (0.1 M, pH~9, Sigma-Aldrich) were used as solvents.

Au NP-immobilization on APTMS functionalized low-e-MIR substrates for SEIRA studies

For the preparation of Au NP immobilized on MIR slides, different concentrations of (3-Aminopropyl) trimethoxysilane (APTMS, 97%, Alfa Aesar) were considered for evaluating the degree of NP immobilization measured by UV-Vis/NIR spectroscopy. APTMS is an agent known for amine functionalization and covalent immobilization of antibodies in high-sensitivity immunoassays [7]. The degree of NP immobilization can be observed by the position and shape of the plasmon band of the Au NP. As a substrate bottom layer, low-e-slides were immersed into a solution of 0.5%, 1% and 1.5% APTMS. For the three APTMS concentrations, two incubation times, 2 h and 24 h, were used. The Au NP immobilization approach with respect to different concentrations of APTMS and incubation times yielded an APTMS concentration of 1% and short incubation time of 2 h being optimal since a small degree of NP aggregation on the substrate was induced. After the incubation time, the silanized slides were rinsed in ultrapure water and soaked into Au NP solution for 4 days and rinsed with ultrapure water after incubation time and allowed to dry in a desiccator. For FTIR-

micro-spectroscopy, 20 µl of the antibody-fluorophore conjugates were dropped-coated onto the Au NP functionalized slide.

UV-Vis/NIR Spectroscopy, Transmission Electron Microscopy (TEM)

The Au NP immobilized on the APTMS-modified substrate were characterized by Atomic Force Microscopy. In order to prove the existence of synthesized Au NP, UV-Vis/NIR Spectroscopy was used for the detection of the plasmon band being characteristic for NP systems. An extinction measurement of the Au NP suspension was performed with a double-beam UV-Vis/NIR spectrophotometer (V-670, Jasco, Germany).

For the determination of the particle dimensions and morphologies, a TEM TECNAI G^2 20 S-TWIN (FEI Company™, USA) was employed. The NP solutions (2 µl) were pipetted onto carbon-coated TEM copper grids (200 mesh, PLANO, Germany) and allowed for air drying. An acceleration voltage of 200 kV was applied for the acquisition of TEM micrographs. Related to the 1×1 inch CCD-chip of the camera an optical magnification ranging from a factor of 20,000 to a factor of 430,000 was used.

Preparation of fluorophore-labeled antibody conjugates

For preparation of fluorophore-labeled Goat Anti-Mouse IgG, 10 mg/ml of the antibody was dissolved in sodium bicarbonate buffer (0.1 M, pH~9, Sigma-Aldrich). The fluorophore Rhodamine B isothiocyanate (RITC) was dissolved in N,N-Dimethylformamide (DMF) at a concentration of 5 mg/ml. Then, a volume of 100 µl of the RITC-solution was pipetted to the antibody solution and allowed to react for 8 h at 4 °C. For the preparation of Goat Anti-Mouse IgG-FITC and Goat Anti-Mouse IgG-SULFO conjugates, the fluorophores Fluorescein 5(6)-isothiocyanate (FITC) and Sulforhodamine B (SULFO) were dissolved in DMF, and pipetted to the Goat Anti-Mouse IgG antibody solution, respectively. After 8 h incubation time at 4 °C in the dark, the conjugates were purified by spin-protocol from unbound dye molecules applying a PD-10 desalting column (Mr~5000 Da, GeHealthcare, Germany). The conjugates were purified by centrifugation for 2 min at 1000×g (Hereaus Megafuge16R, ThermoScientific, USA). Sodium bicarbonate buffer (0.1 M, pH~9) was used as eluent. No adjustment to the alkaline milieu was necessary for the incubation of the antibodies with NP suspensions since both antibodies and fluorophores were already prepared under alkaline conditions along with the respective coupling procedures.

MALDI-TOF-MS of the fragmented fluorophore-antibody conjugates

For Matrix-Assisted Laser Desorption/Ionization Mass Spectrometry (MALDI-TOF-MS), trypsin was used as digestive enzyme for the fragmentation of the antibody conjugates. For the antibody digestion, 20 μg of lyophilized trypsin (Sigma) was dissolved in 20 μl of hydrochloric acid (1 mM, pH~3.0) and ammonium bicarbonate digestion buffer (100 mM, pH~8.5). For an antibody protein concentration of 10 μg (reference), 0.5 g trypsin was used and diluted at 1:20 w/w. Trypsin was pipetted at a concentration of 1:100 w/w the conjugate suspensions. Incubation was performed at 37 °C for 2 to 8 h. Purification was performed with ZebaSpin columns (Pierce, Belgium). For MALDI measurements, the samples were embedded in a sample matrix that consisted of trans-3.5-dimethoxy-4-hydroxysinapin acid (>99%, Protea, USA). The digested samples, that is, the reference standard and the antibody conjugates were mixed with the sample matrix which consisted of a mixture containing acetonitrile (ACN, 99.8%, anhydrous, Sigma Aldrich) and trifluoracetic acid (TFA, 99.5%, Sigma) with a molar ratio of ACN/TFA (70/30 Vv), respectively. Measurements were performed with a AutoFlex III MALDI-TOF mass spectrometer (Bruker Daltonik, Germany) using an UV-laser (λ= 337 nm) with a pulse-length of 3 nm and an acceleration voltage of 20 kV. Mass spectra of fragmented antibody conjugates were examined in the region from 340 m/z to 600 m/z. These studies were performed in order to check the existence of molecule ions referring to uncoupled dye molecules in the conjugate.

Additional information on **Results and discussions**

Characterization of the Au NP suspension for the preparation of SEIRA substrates

Figure S-1 depicts the extinction spectrum of the Au NP suspension. The characteristic position of the plasmon resonance band of the colloidal Au is located at 530 nm. The insets show the TEM images of the Au colloid, and the size distribution of the Au NP is determined to range from 20 nm to 40 nm (Fig. S-1). Au NPs show a spherical-shaped to slightly rod-shaped morphology.
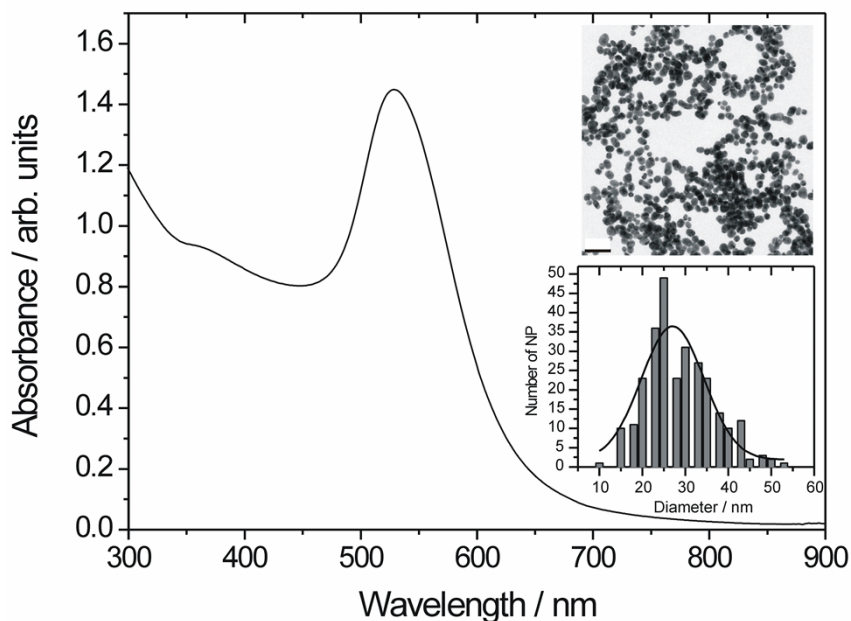
Fig. S-1. Extinction spectrum of the Au NP suspension with the corresponding TEM micrographs (scale bars: 100 nm).

MALDI-TOF-MS analysis of the fragmented fluorophore-antibody conjugates

The detection of covalently-linked molecules allows to reveal the existence of uncoupled dye molecules in the conjugate which can be identified by their molecule ions [8, 9] via mass spectroscopy. Figure S-2 shows the MALDI data of the fragmented (A) antibody reference Goat Anti-Mouse IgG, (B) antibody-FITC conjugate, (C) antibody-RITC conjugate and (D) antibody-SULFO conjugate.

The m/z values for the fluorophores FITC, RITC and SULFO correspond to their molecular weights that lie at 389.38 m/z, 536.08 m/z and 577.11 m/z. The obtained MALDI spectra prove that the mono-isotopic molecule ions of the fragmented antibody and that no molecule ions originating from the coupled dyes are detectable which gives a qualitative evidence of a successful coupling procedure of the fluorophores to the antibody [10]. This is important in case of a distinct and reliable SEIRA characterization of labeled antibodies only whose MIR signatures are studied for immunoassay applications.
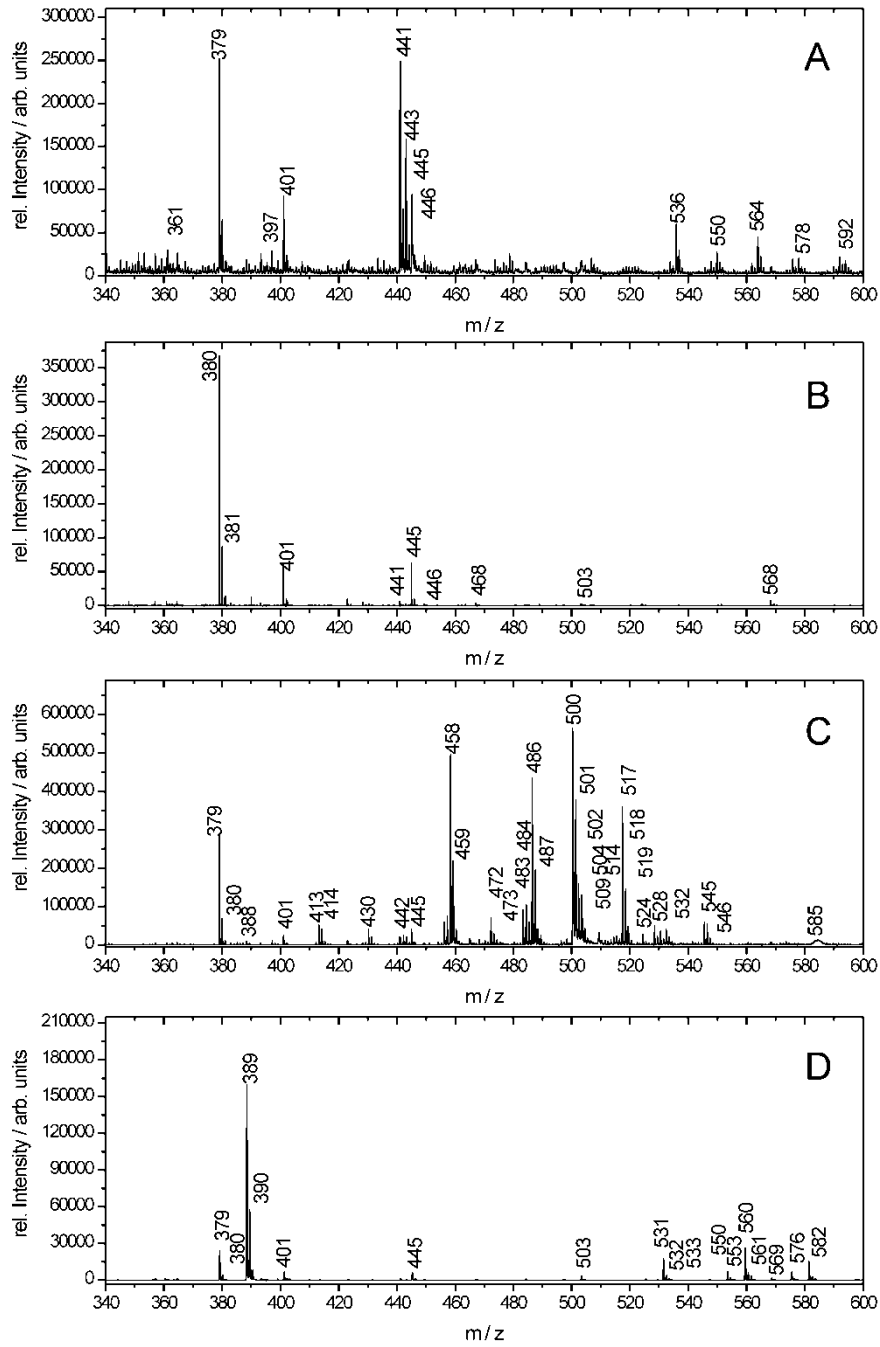
Fig. S-2. MALDI-TOF-MS spectra of the fragmented (A) Goat Anti-Mouse IgG antibody standard, (B) antibody-FITC conjugate, (C) antibody-RITC conjugate and (D) antibody-SULFO conjugate.

Table S-1. Band assignments of the Infrared spectra and enhanced infrared spectra (for Au NP) of the label components Goat Anti-Mouse IgG, here as 'Goat' ([a]ref.[11, 12]), FITC ([b]ref.[13, 14]) and Goat-FITC ([c]ref. [12, 14-18]). **Enhanced modes** and **new emerging bands** are highlighted in **bold**. Abbreviations: δ deformation, ν stretching, *s,as* (as)symmetrical.

Goat	[a]assignments	Au NP-Goat	[a]assignments	FITC	[b]assignments	Au NP-FITC	[b]assignments	Goat-FITC	[c]assignments	Au NP-Goat-FITC	[c]assignments	Mouse IgG	assignments	Au NP Mouse IgG	assignments
1064	ν C-O-C	1250	νas PO2-	982	ν C-O-C	**1180**	**ν COH**	1103	ν C-O-C	1227	ν C-O	1022	ν C=O	**1003**	**ν C=O**
1242	νas PO2-	1334	ν C=N	1105	ν C-O-C	**1203**	**ν C-O**	1165	δ CH	1253	νas PO2-	1057	ν C=O	**1073**	**ν C=O**
1088	δ CH, ν C-O-C	1388	δ CH3	1176	δ C-OH	**1304**	**ν C-O**	1242	νas PO2-	1347	xanthene ring ν C-C	1173	ν C-OH	**1173**	**ν C-OH**
1358	δ CH3	1442	δas CH3	1247	ν C-O	1388	ν C=N, ν C-C	1334	xanthene ring ν C-C	**1399**	**δ N=O**	1344	ν C=N	**1344**	**ν C=N**
1450	δas CH3	**1527**	**Amid II, δ N-H, ν C-N**	1313	ν C=N	**1458**	**δas CH3**	1388	ν C=N, ν C-C	1460	νas CH3	1393	ν C=N	**1441**	**δas CH3**
1535	Amid II, δ N-H, ν C-N	1628	Amid I (ν C=O, δ CN, δ N-H)	1388	ν C=N, ν C-C	1496	central ring breathing ν C-C	1450	νas CH3	**1527**	**δ CH3**	1441	δ NH	**1597**	**arom. ν C-C**
1635	Amid I (ν C=O, δ CN, δ N-H), arom. ν C-C	**2870**	**νs CH3**	1450	δas CH3	**1597**	**arom. ν C-C**	1525	ν C=N, arom. ν C-C	1597	arom. ν C-C	1641	Amid I (ν C=O, δ CN, δ N-H), arom. ν C-C	1641	Amid I (ν C=O, δ CN, δ N-H), arom. ν C-C
1736	ν C=O	**2931**	**νas CH2**	1496	central ring breathing ν C-C	1738	ν C=O	1643	arom. ν C-C	**1643**	**arom. ν C-C**	3340	ν NH	**3278**	**ν NH**
2877	νs CH2	3062	νas C=C-H2	1527	ν C=N, arom. ν C-C	**1886**	**ν CO**	1738	ν C=O	3286	ν OH			**3415**	**ν NH**
2962	νas CH2	3109	νas C=C-H2	1652	arom. ν C-C	**2029**	**ν CO**	2885	νs CH3					**3492**	**ν NH**
3070	νas N-CH3	**3278**	**ν NH**	1738	ν C=O	**2098**	**ν CO**	2931	νas CH2						
3294	ν NH	**3649**	**ν NH**	2953	νas CH3			3070	νas C=C-H2						
		3720	**ν OH**					3286	ν NH						
								3633	ν NH						
								3720	ν OH						

Table S-2. Band assignments of the Infrared spectra and enhanced infrared spectra (for Au NP) of the label components Goat Anti-Mouse IgG, here as 'Goat' ([a]ref.[11]), RITC ([b]ref.[13, 14]) and Goat-RITC ([c]ref. [12, 14-18]). **Enhanced modes** and **new emerging bands** are highlighted in **bold**. Abbreviations: δ deformation, ν stretching, *s,as* (as)symmetrical.

RITC	[b]assignments	Au NP-RITC	[b]assignments	Goat-RITC	[c]assignments	Au NP-Goat-RITC	[c]assignments
964	ν C=O	**964**	**ν C=O**	**976**	**ν C=O**	1180	δ C-OH
976	ν C=O	**1010**	**ν C=O**	1026	ν C=O	**1334**	**xanthene ring ν C-C**
1056	ν C=O	**1072**	**ν C=O**	1080	ν C=O	**1390**	**δ CH$_3$**
1149	ν C=O	**1149**	**ν C=O**	1134	δ CH	**1581**	**arom. ν C-C**
1172	δ C-OH	**1172**	**δ C-OH**	1180	ν COH	**1639**	**arom. ν C-C**
1273	ν C-OH	**1211**	**ν C-O**	**1242**	**ν$_{as}$ PO$_2^-$**	2869	ν$_s$ CH$_3$
1342	xanthene ring ν C-C	**1273**	**ν C-OH**	1273	ν C-OH	2931	ν$_{as}$ CH$_2$
1412	δ N=O	1327	xanthene ring ν C-C	1334	xanthene ring ν C-C	3078	ν$_{as}$ C=C-H$_2$
1453	δ$_{as}$ CH$_3$	**1381**	**ν C=N, ν C-C**	**1412**	**δ N=O**	3204	ν OH
1520	δ CH$_3$, ν C=N, arom. ν C-C	**1412**	**δ N=O**	1456	δ$_{as}$ CH$_3$	**3286**	**ν NH**
1589	arom. ν C-C	**1453**	**δ$_{as}$ CH$_3$**	1496	central ring breathing ν C-C		
1638	Amid I (ν C=O, δ CN, δ N-H), arom. ν C-C	**1496**	**central ring breathing ν C-C**	**1589**	**arom. ν C-C**		
1743	ν C=O	**1589**	**arom. ν C-C**	1647	arom. ν C-C		
2941	ν$_{as}$ CH$_2$	**1666**	**ν C=O**	1751	ν C=O		
		1743	**ν C=O**	1813	ν C=O		
		2665	**ν C-H**	2869	ν$_s$ CH$_3$		
		2941	**ν$_{as}$ CH$_2$**	2931	ν$_{as}$ CH$_2$		
		3224	ν NH	3076	ν$_{as}$ N-CH$_3$		
				3286	ν NH		

Table S-3. Band assignments of the Infrared spectra and enhanced infrared spectra (for Au NP) of the label components Goat Anti-Mouse IgG, here as 'Goat (ref[11]), SULFO ([b]ref.[13, 14]), and Goat-SULFO ([c]ref. [12, 14-18]). **Enhanced modes** and **new emerging bands** are highlighted in **bold**. Abbreviations: δ deformation, ν stretching, *s,as* (as)symmetrical.

SULFO	[b]assignments	Au NP-SULFO	[b]assignments	Goat-SULFO	[c]assignments	Au NP-Goat-SULFO	[c]assignments
972	ν C-O-C	**972**	**ν C-O-C**	972	**ν C-O-C**	**1034**	**δ CH**
1034	δ CH	**1034**	**δ CH**	1034	**δ CH**	**1080**	**ν C-O-C**
1080	ν C-O-C	**1080**	**ν C-O-C**	1080	**ν C-O-C**	**1126**	**xanthene ring ν C-C**
1134	δ CH, ν C-C	1188	ν C-C	1126	xanthene ring ν C-C	**1196**	**ν C-C**
1196	ν C-C	1226	xanthene ring ν C-C	1188	ν C-C	1242	ν C-O
1242	ν C-O	1327	xanthene ring ν C-C	**1242**	**ν C-O**	**1350**	**ν N=O**
		1396	ν C=N	1273	ν C-OH	1412	νs CH2
1342	xanthene ring ν C-C	1496	central ring breathing	**1342**	**xanthene ring ν C-C**	1458	δ NH
1419	νs CH2			1412	νs CH2	1504	δ NH, ν C-O
1466	νas CH3	**1535**	**δ CH3**	1466	νas CH3	**1612**	**δ NH2**
1535	arom. ν C-C	**1581**	**arom. ν C-C**	1535	δ CH3	1658	Amid I (ν C=O, δ CN, δ N-H), arom. ν C-C
1597	arom. ν C-C	**1643**	**arom. ν C-C**				
1651	Amid I (ν C=O, δ CN, δ N-H), arom. ν C-C	**1705**	**ν C-O**	**1597**	**arom. ν C-C**	1844	ν C=O
1874	ν C-O	1874	ν C-O	1658	Amid I (ν C=O, δ CN, δ N-H), arom. ν C-C	1928	ν C=C
2870	νs CH3	**2870**	**νs CH3**	1844	ν C=O	**2870**	**νs CH3**
2970	νas CH3	3186	arom. ν C-C + δ CH3	1928	ν C=C	2931	ν C=C
3217	ν NH	3325	ν NH	**2870**	**νs CH3**	2977	νas CH3
3278	ν NH, OH	3780	ν OH	2977	νas CH3	3278	ν NH
3355	ν NH			**3278**	**ν NH**		
3425	ν NH						
3726	ν OH						

Studies on complex biolabels in the Amide I/II and ester regions

If we compare the IR spectra of all bioconjugates we can predominantly figure out spectral features in the region of C–O stretches that appear as two or more bands in the region 1300–1000 cm^{-1} along with fluorophore specific modes. The SEIRA signatures display different shapes of modes along with shifted bands and enhanced spectral features. From these observations we infer that the SEIRA technique can contribute to the development and characterization of new complex SEIRA-based biolabels which in turn can be implemented for prospective bio-assay approaches. With the SEIRA readout we open new opportunities for discriminating multiple biolabels that entail similar features compared to conventional IR data, but are definitely unique. This enforces the discrimination capabilities between analyte molecules (antigens) that may couple to these SEIRA biolabels.
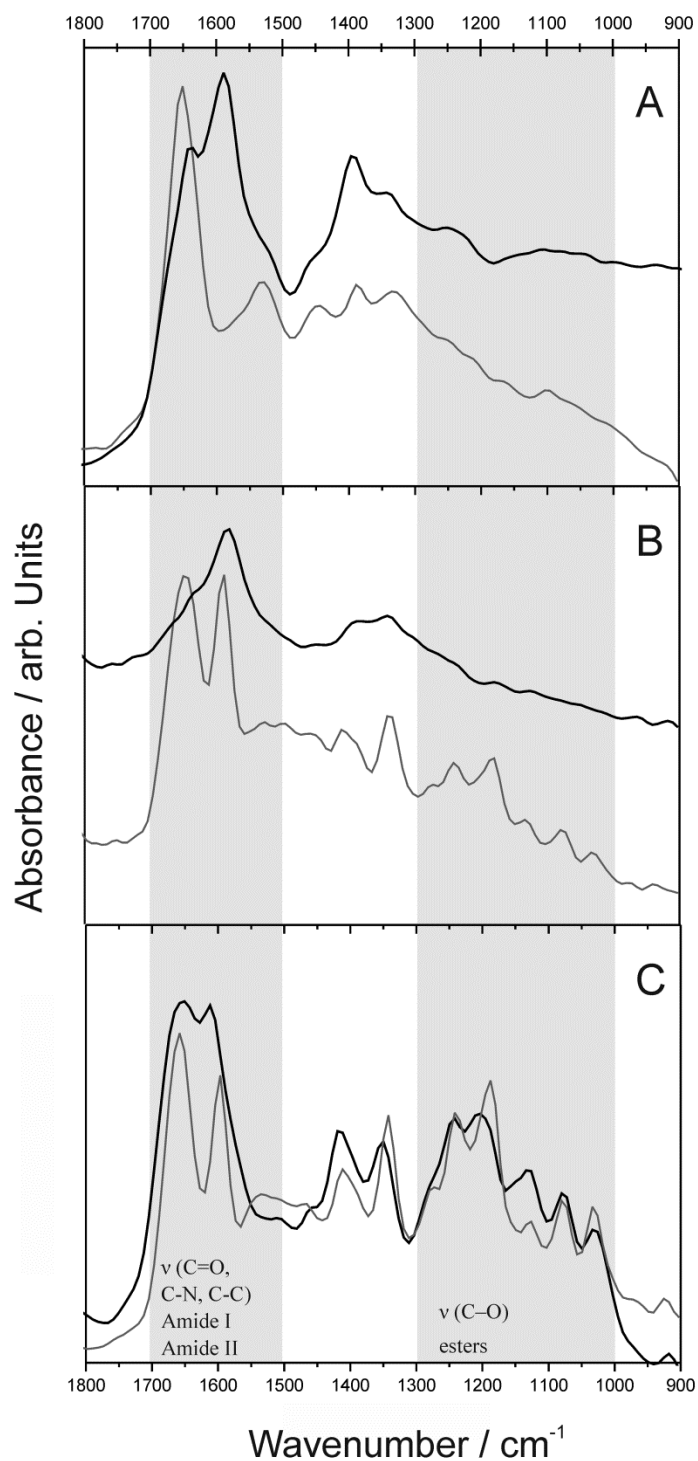
Fig. S-3. Mid-infrared spectra (gray lines) and SEIRA signatures (black lines): (A) antibody-FITC conjugate and Au NP- antibody-FITC biolabel, (B) antibody-RITC conjugate and Au NP-antibody-RITC biolabel, and (C) antibody-SULFO conjugate and Au NP-antibody-SULFO biolabel. For studies on molecular structures of complex biologically relevant samples such as complex biolabels the Amide I/II and ester regions are considered (highlighted).   .

References

1   T. A. Laurence, G. B. Braun, N. O. Reich and M. Moskovits, *Nano Letters*, 2012, **12**, 2912-2917.

2   E. J. Blackie, E. C. L. Ru and P. G. Etchegoin, *Journal of the American Chemical Society*, 2009, **131**, 14466-14472.

3   R. F. Aroca and D. J. Ross, *Appl. Spectrosc.*, 2004, **58**, 324A-338A.

4   A. Hartstein, J. R. Kirtley and J. C. Tsang, *Phys. Rev. Lett.*, 1980, **45**, 201-204.

5   M. Osawa and K.-i. Ataka, *Surf. Sci.*, 1992, **262**, L118-L122.

6   G. Dovbeshko, O. Fesenko and A. Nazarova, *Journal of Physical Studies*, 2006, **10**, 127-134.

7   C. K. Dixit, S. K. Vashit, B. D. MacCraith and R. O'Kennedy, *Nat. Protoc.*, 2011, **6**, 439-445.

8   M. Barber, R. S. Bordoli, R. D. Sedgwick and A. N. Tyler, *J. Chem. Soc.-Chem. Comm.*, 1981, 325-327.

9   M. Karas and F. Hillenkamp, *Anal. Chem.*, 1988, **60**, 2299-2301.

10   M. Adamczyk, A. Buko, Y.-Y. Chen, J. R. Fishpaugh, J. C. Gebler and D. D. Johnson, *Bioconjugate Chemistry*, 1994, **5**, 631-635.

11   F. S. Parker, *Applications of Infrared, Raman, and Resonance Raman Spectroscopy in Biochemistry*, Plenum Press New York and London, 1983.

12   F. S. Parker and D. M. Kirschenbaum, *Nature*, 1960, **187**, 386-388.

13   M. Majoube and M. Henry, *Spectrochim. Acta, Part A: Mol. Spectrosc.*, 1991, **47**, 1459-1466.

14   R. Markuszewski and H. Diehl, *Talanta*, 1980, **27**, 937-946.

15   J. A. Seelenbinder, C. W. Brown, P. Pivarnik and A. G. Rand, *Anal. Chem.*, 1999, **71**, 1963-1966.

16   C. W. Brown, Y. Li, J. A. Seelenbinder, P. Pivarnik, A. G. Rand, S. V. Letcher, O. J. Gregory and M. J. Platek, *Anal. Chem.*, 1998, **70**, 2991-2996.

17   T. Ohishi, *J. Non-Cryst. Solids*, 2003, **332**, 80-86.

18   Y.-F. Fang, Y.-P. Huang, D.-F. Liu, Y. Huang, W. Guo and D. Johnson, *J. Environ. Sci.*, 2007, **19**, 97-102.